Short Communication

Aquaporin-4 Positron Emission Tomography Imaging of the Human Brain: First Report

Yuji Suzuki, MD, PhD, Yukihiro Nakamura, PhD, Kenichi Yamada, MD, PhD, Vincent J. Huber, PhD, Mika Tsujita, PhD, Tsutomu Nakada, MD, PhD, FAAN

From the Center for Integrated Human Brain Science, Brain Research Institute, University of Niigata.

ABSTRACT

BACKGROUND AND PURPOSE

Aquaporin 4 (AQP-4) is the most abundant aquaporin isoform in the brain. Alterations in its expression and distribution have been correlated with the progression of several clinical disorders; however, the specific roles of AQP-4 in those disorders are not well understood. Visualizing AQP-4 in vivo is expected to provide fresh insights into its roles in disease pathology, as well as aiding the clinical assessment of those disorders.

METHODS

We developed a ^{11}C-labeled analogue of the AQP-4 ligand TGN-020 (2-nicotinamido-1,3,4-thiadiazole) suitable for in vivo positron emission tomography (PET) imaging.

RESULTS

In the present study, we report the first PET images of AQP-4 in the human brain. The results unequivocally demonstrated a specific distribution pattern for AQP-4 within the brain, namely, the subpial and perivascular endfeet of astrocytes. The choroid plexus, where both AQP-4 and AQP-1 are expressed, also showed substantial uptake of the ligand.

CONCLUSIONS

Based on these initial results, we believe [^{11}C]TGN-020 PET will be valuable in determining the role of AQP-4 in disease progression, and for the clinical assessment of water homeostasis under various settings.

Keywords: Human, aquaporin 4, positron emission tomography (PET), ^{11}C, TGN-020.

Acceptance: Received December 21, 2011, and in revised form February 15, 2012. Accepted for publication February 17, 2012.

Correspondence: Address correspondence to Tsutomu Nakada, MD, PhD, FAAN, Center for Integrated Human Brain Science, Brain Research Institute, University of Niigata 1 Asahimachi, Niigata 951–8585, Japan. E-mail: tnakada@bri.niigata-u.ac.jp.

Disclosure: The authors state that they have no conflict of interest to disclose.

J Neuroimaging 2013;23:219-223.
DOI: 10.1111/j.1552-6569.2012.00704.x

Introduction

Aquaporin 4 (AQP-4) represents the isoform of the membrane integral water channel aquaporin family that is most abundant within the brain. Its distribution is unique and is restricted to the subpial and perivascular endfeet of astrocytes.[1,2,3] While this protein is thought to be vital to normal physiological brain functions such as neural-flow coupling,[4] evidence continues to accumulate suggesting AQP-4 also plays a significant role in the pathophysiology of various brain diseases, from epilepsy to Alzheimer's disease.[5-9] However, the exact roles AQP-4 plays in normal and pathological conditions have not been clearly elucidated.

In order to further advance our understanding of the neurophysiology and neuropathology of AQP-4, it would be useful to monitor changes to its expression and distribution in response to a variety of situations. The development of a *noninvasive* clinical quantitative imaging method for depicting AQP-4 distribution in the brain in vivo is essential for initiating such a study. Unfortunately, very few AQP-4 ligands have been reported that could be used as the basis for such a radiotracer. Recently, 2-nicotinamido-1,3,4-thiadiazole (TGN-020) was identified in our laboratory as inhibiting AQP-4 mediated water transport in vitro,[10] and was subsequently found to reduce the formation of cerebral edema in rodent ischemia models.[9] Introducing a ^{11}C radiolabel into that compound ([^{11}C]TGN-020) allowed us to generate small animal PET images in wild type and AQP-4 null mice in vivo, where differential uptake was observed in tissues having known AQP-4 expression.[11] That study confirmed that [^{11}C]TGN-020 possesses suitable qualities as an AQP-4 ligand to be used in human PET imaging, despite little apparent selectivity over aquaporin 1 (AQP-1).

Accordingly, we advanced our study to clinical investigation, after having performed all prerequisite toxicological studies, and present here the first report of an AQP-4 PET study in human volunteers.

Materials and Methods

Ligand Preparation

Radio synthesis

Tracer radiosynthesis was described in detail previously,[11] and modified as follows: [^{11}C]TGN-020 was prepared using a TRACERlab FXC Versatile Automated Synthesizer (GE

Healthcare, Schenectady NY, USA). $^{11}CO_2$ was produced using a PETtrace cyclotron (GE Healthcare), and was trapped at −100 °C prior to usage. An aliquot of 1.6 M *n*-BuLi (0.1 mL, 0.16 mmol) was added directly to a stirred solution of 3-bromopyridine (0.025 mL, 0.26 mmol) in dry ether (0.5 mL) at −70 °C under helium. The resulting solution was stirred at −70 °C for 30 min, at which time $^{11}CO_2$ (approximately 60.0 GBq) was bubbled through the reaction mixture. Subsequently, unlabeled dry CO_2 was added to quench any active lithium species. The resulting mixture was heated and an aliquot of 1 M HCl (0.3 mL, 0.3 mmol) was added. The resulting mixture was evaporated under a dry-helium stream. Solutions of 2-amino-1,3,4-thiadiazole (0.0050 g, 0.050 mmol) and 1-ethyl-3-(3-dimethylaminopropyl) carbodiamide (0.010 g or 0.053 mmol) in dry DMF (0.6 mL) were then added to the residue. The resulting mixture was stirred for 5 minutes and evaporated under a stream of dry helium at elevated temperature. The residue was dissolved in 0.01 M NaOH (0.8 mL) and purified by semi-preparative HPLC. Composition of the isolated product was confirmed by analytical HPLC against an authentic TGN-020 standard. Aqueous sodium bicarbonate (7% $NaHCO_3$, 5 mL) was added to the isolated product to give a pH in the range of 6–8. Routine quality control measurements of the solutions for human injection consisted of pH, chemical purity, radiochemical purity, and endotoxin tests. All [^{11}C]TGN-020 samples used in this study had chemical and radiochemical purities >95%, with radiochemical yields between 300–500 MBq.

Toxicology

Toxicity and mutagenicity tests were performed by the Mitsubishi Chemical Safety Institute Ltd (Tokyo, Japan). The acute toxicity of TGN-020 was assayed in Crj:CD(SD) rats, where the compound was injected into the tail vein of 6-week-old animals (five each male and female rats having a weight range of 114–132 and 89–110 g, respectively) in 1, 10, and 100 mg/kg doses. The dosage range was selected such that the lowest dose was >1,000 times the estimated administration amount of [^{11}C]TGN-020 (ca. 1 μg/kg, 200 MBq of [^{11}C]TGN-020). No mortality was observed following TGN-020 administration at any of the doses, and all test animals showed body-weight gains comparable to that of control rats during the 14-day post-treatment observation period. Treated rats were then sacrificed. Postmortem histopathological examination of brain (cerebrum, cerebellum), heart, lung, liver, stomach, spleen, kidney, eye, and tail (treated site) tissues showed no abnormalities.

TGN-020 was tested for mutagenicity in the Ames test using five histidine-requiring strains of Salmonella typhimurium (TA98, TA100, T1535, and T1537) and *Escherichia coli* (WP2uvrA-), with a mixture of rat liver enzymes on agar lacking histidine (S9 mixture). The compound was tested at doses between 1.22 and 5,000 g/plate using the standard method.[12] No mutagenic activity was observed in relation to TGN-020.

Post-decay acute toxicity of [^{11}C]TGN-020 was evaluated in mice as follows. Three lots of [^{11}C]TGN-020 were prepared. After complete decay out of ^{11}C, the compound was injected into the tail veins of 8–10-week-old mice ($n = 3$ for each lot, 25–30 g body weight) at doses of 1.0–2.0 mg/kg body weight, which was >1,000 times the anticipated human administration dose. Animals were monitored for clinical manifestations during a 2-week observation period, and were weighed daily. All mice in the test group showed normal body weight gains compared to that of the control group (injected saline), and no toxicological effects were observed.

Affinity comparison

Xenopus oocytes, reagents, and solutions were prepared as previously described.[13] cDNA encoding human Aquaporin 1 (hAQP-1) was purchased from ATCC biological resource center (Manassas, Virginia), GenBank number BC022486. cDNA encoding the human Aquaporin 4-M23 isoform was cloned by reverse-transcription polymerase chain reaction (RT-PCR), and the first-strand cDNA was synthesized from human cerebellum total RNA by using the Advantage RT-for-PCR Kit (Clontech, Otsu, Japan). The oligonucleotide PCR primers were designed based on published hAQP-4M23 sequences.[14] Full-length AQP1 or AQP4-M23 cRNA was subcloned into the pSP35T expression vector for Xenopus oocyte.[15] The resulting cRNA was sequenced, and was found to be in agreement with literature reports.[14]

The in vitro AQP inhibition assay was described in detail previously,[13] and modified as follows: Five to six oocytes along with modified Barth's medium (MBS, 450 mL) were transferred to a 24 well-polystyrene plate (Costar 3526) to which an aliquot (50 mL) of ligand stock solution (0.2 mM in 1% DMSO containing MBS) or a blank (1% DMSO in MBS) had been added. Oocytes were incubated at 20 °C for 30 minutes. Prior to imaging, the plate was transferred to an SZX16 zoom microscope (Olympus Corporation, Tokyo, Japan) fitted with a DP26 digital camera (Olympus) and a MATS-5555 temperature controlled stage (Tokai Hit, Fujinomiya, Japan) set at 24 °C. Hypotonic shock was initiated by introducing an equimolar ligand solution or blank in 0.1% aqueous DMSO, also maintained at 24 °C. Single-well images were captured in 15-seconds intervals for 250 seconds following the addition of hypotonic medium. Experiments were performed using acetazolamide as a positive control.

Images were transferred to a personal computer and the hypotonic response of individual oocytes was evaluated as previously described.[13]

Human Brain PET

Subjects

Five healthy male volunteers (age 20–52 years) participated in this study. Informed written consent was obtained for all volunteers. Studies were performed according to the human research guidelines of the Internal Review Board of University of Niigata. This project was registered at the UMIN Clinical Trials Registry as UMIN000005626 (http://www.umin.ac.jp/ctr/index.htm).

PET imaging

PET imaging was performed using a combined PET/CT scanner (Discovery ST Elite, GE Healthcare) with a 15 cm field of view (FOV) positioned in the region of the cerebrum and

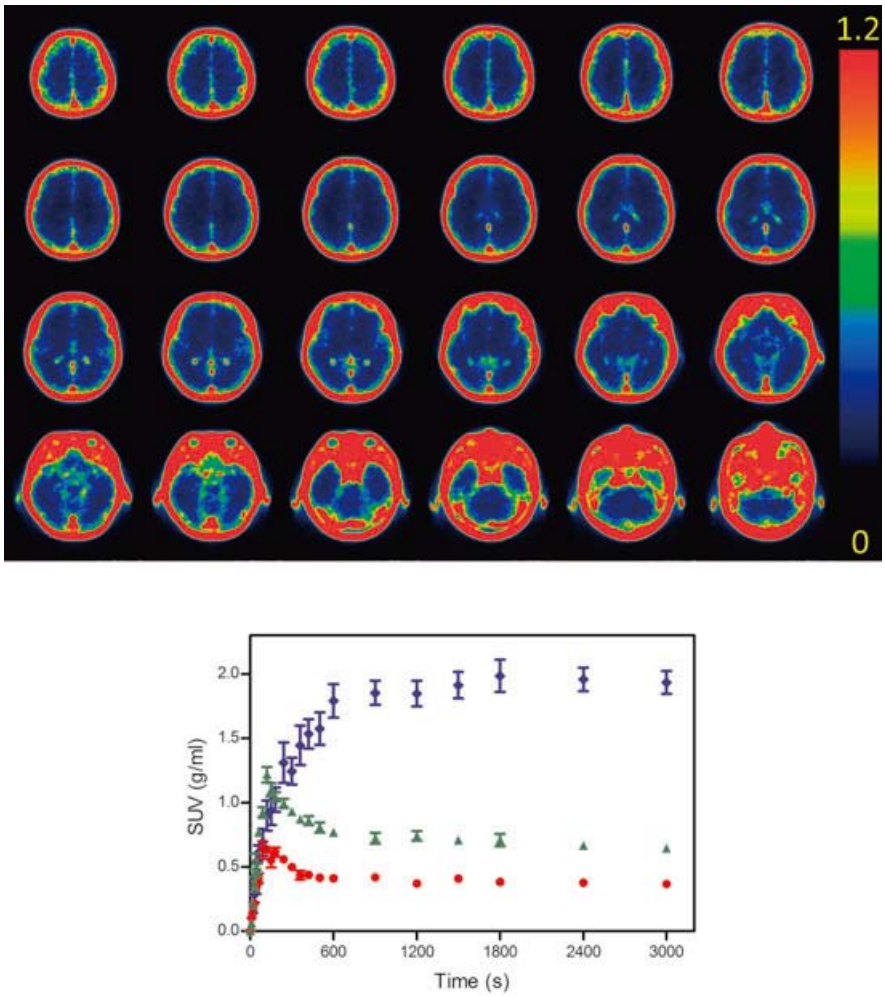

Fig 1. Upper: Representative ^{11}C-TGN-020 PET images of normal human brain images are constructed based on the frames acquired 15–60 minutes post-injection. All five subjects studied exhibited virtually identical findings. Images are color coded according to standardized uptake value (SUV) of each pixel in the range of 0–1.2. Over ranged (1.2 > SUV) pixels are expressed as red. Strongest uptake was seen in the skull and within large veins and dural sinuses. Radioactivities within large veins and dural sinuses are believed to reflect AQP-1 of red cells. The cause for strong uptake within the skull remains to be elucidated. Lower: Time-activity curves of uptake in SUV of three representative regions. Red circle: cortex, green triangle: choroid plexus, blue diamond: skull. Data are shown as mean SUV ± standard error of means (SEM).

cerebellum. To correct for photon attenuation, a low-dose CT scan was acquired in helical mode with the following parameters: 120 kV, 50 mA, 0.8 seconds per tube rotation, slice thickness of 3.75 mm with internals of 3.27 mm, pitch of 0.875, and a table speed of 17.5 mm/rotation. After an intravenous injection of 120–240 MBq [^{11}C]TGN-020 (1.5–3.5 MBq/kg body weight) for 2 minutes by syringe pump (PHD2000, HARVARD, Massachusetts, USA), PET emission data were acquired over 60 minutes in three-dimensional list mode with an 25.6 cm axial FOV and sorted into 25 time frames (6 × 10, 6 × 30, 6 × 60, 4 × 300, and 3 × 600 seconds). All PET emission scans were normalized for detector inhomogeneity and corrected for random coincidences, dead time, scattered radiation, and photon attenuation. The 25 frames of the dynamic-emission scans were reconstructed using 3D-OSEM (Ordered-Subset Expectation Maximization) with two iterations and 28 subsets to obtain superior visual quality images, allowing manual definition of regions of interest (ROIs). For the reconstruction algorithms, the data were collected in a 128 × 128 × 47 matrix with a voxel size of 2.0 × 2.0 × 3.27 mm.

The CT and PET image data were transferred to a Xeleris 1.1 workstation (GE Healthcare) for PET data analysis. Manually defined ROIs on the attenuation corrected axial images and CT images were used to obtain the time-activity data in each scan for each subject. The tissue activity concentration in each ROI was expressed as the standardized uptake value (SUV), corrected for the subject's body weight and administrated dose of radioactivity.

Results and Discussion

No acute TGN-020 toxicity was identified at doses >1,000 times the maximum [^{11}C]TGN-020 administration levels, and all test animals were absent of abnormalities in the postmortem histopathological examination. Moreover, TGN-020 was negative in the Ames mutagenicity test, and post-decay [^{11}C]TGN-020 also showed no acute toxicity.

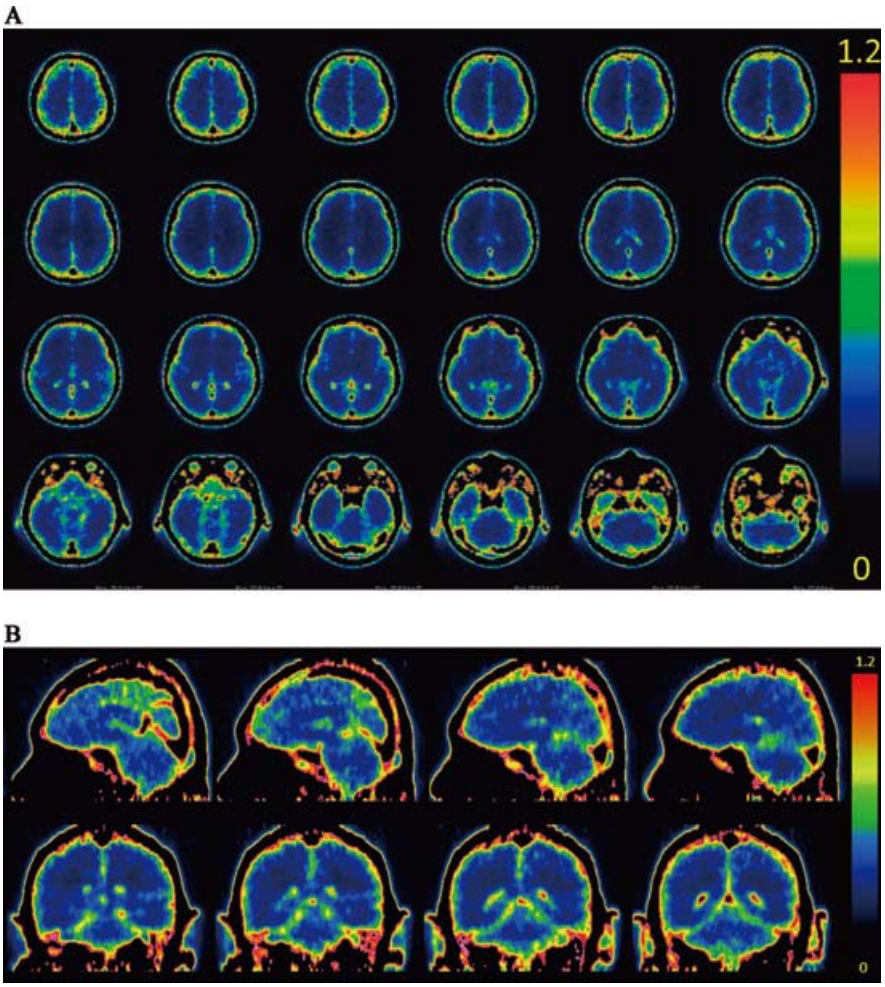

Fig 2. Images constructed with filling pixels, which showed the SUV over 1.2, in black. Axial images based on identical data [Fig 1 (A)] and representative images of sagittal and coronal views (B). All images were constructed based on the frames acquired 15–60 minutes post injection. Distribution of radioactivities within the brain are highly consistent with known distribution of AQP-4, namely, subpial, and perivascular endfeet of astrocytes. Choroid plexus, where both AQP-4 and AQP-1 are known to be significantly expressed, also showed significant uptake.

Evaluation of TGN-020's effect on AQP-1 mediated water transport in vitro showed that it has a similar inhibitory effect as found for AQP-4.[10] Following a hypotonic shock, the transmembrane water flux of xenopus oocytes expressing human AQP-1 was reduced by $56 \pm 9\%$ when incubated with 20 μM TGN-020. This inhibition was comparable to that found for the same ligand and human AQP-4, which was found to have a $67 \pm 6\%$ water flux reduction.[10] The similar inhibitory level at identical concentrations suggested [^{11}C]TGN-020 would not effectively discriminate between AQP-1 versus AQP-4 isoforms in the PET imaging study.

Representative axial PET images constructed from the frames of 15–60 minutes post-injection with steady tissue uptake level are shown along with time activities of uptake in SUV within the representative structures in Figure 1. There is a first pass-effect observed within the first 10 minutes, followed by steady state levels for cortex and choroid plexus in the frame of 15–60 minutes. The strongest uptake was seen in the skull and within large veins and dural sinuses. Since AQP-1 expression is suppressed within vessels of the brain,[16] uptake within large veins and dural sinuses was believed to reflect AQP-1 of red cells. Since adult brain does not show strong hematopoietic activities and, hence, there would be few red cells, if any, within the skull, the cause for strong uptake within the skull remains to be elucidated.

In order to make visual inspection of ligand distribution within the brain easier, significantly high-SUV area within the skull, large veins, and dural sinuses were digitally eliminated, and reconstructed images were presented in Figure 2A. Representative coronal and sagittal images were also shown in Figure 2B. Distribution of ligand within the brain was highly consistent with known distribution of AQP-4, namely, subpial, and perivascular endfeet of astrocytes and choroid plexus. The latter is known to significantly express both AQP-4 and AQP-1.[17] Single cell ependymal line along ventricular walls was not well visualized in spite of known high-AQP-4 expression,[3] presumably due to the limit of spatial resolution of our PET system.

Future studies will be necessary to extend this work to full-body imaging, particularly of the skeletal muscles, which also

have a selective distribution of AQP-4, and to identify the reason for significant radio-ligand uptake in the skull. Nevertheless, these results clearly demonstrate the potential for using [^{11}C]TGN-020 as a means of visualizing AQP-4 distribution in vivo, and present an image of the brain that has never been seen before. Considering the potential role of AQP-4 in the pathogenesis of neuromyelitis optica (NMO), clinical applications of AQP-4 PET in neurology appears to be eminent.[18]

The work was supported by grants from the Ministry of Education, Culture, Sports, Science, and Technology (Japan), and University of Niigata. The study was in part presented at XXVth International Symposium on Brain Blood Flow, Metabolism, and Function & Xth International Conference on Quantification of Brain Function with PET, Barcelona, Spain May 25-28, 2011.

References

1. Jung JS, Bhat RV, Preston GM, et al. Molecular characterization of an aquaporin cDNA from the brain: Candidate osmoreceptor and regulator of water balance. *Proc Natl Acad Sci USA* 1994;91:13052-13056.
2. Amiry-Moghaddam M, Ottersen OP. The molecular basis of water transport in the brain. *Nat Rev Neurosci* 2003;4:991-1001.
3. Mobasheri A, Marples D, Young IS, et al. Distribution of the AQP-4 water channel in normal human tissues. *Channels* 2007;1:29-38.
4. Kitaura H, Tsujita M, Huber VJ, et al. Activity-dependent glial swelling is impaired in aquaporin-4 knockout mice. *Neurosci Res* 2009;64:208-212.
5. Lee TS, Eid T, Mane S, et al. Aquaporin-4 is increased in the sclerotic hippocampus in human temporal lobe epilepsy. *Acta Neuropathol* 2004;108:493-502.
6. Nakada T. Neuroscience of water molecules: A salute to Professor Linus Carl Pauling. *Cytotechnol* 2009;59:145-152.
7. Verkman AS. Aquaporins: Translating bench research to human disease. *J Exp Biol* 2009;212:1707-1714.
8. Moftakhar P, Lynch MD, Pomakian JL, et al. Aquaporin expression in the brains of patients with or without cerebral amyloid angiopathy. *J Neuropathol Exp Neurol* 2010;69:1201-1209.
9. Igarashi H, Huber VJ, Tsujita M, et al. Pretreatment with a novel aquaporin 4 inhibitor, TGN-020, significantly reduces ischemic cerebral edema. *Neurol Sci* 2011;32:113-116.
10. Huber VJ, Tsujita M, Nakada T. Identification of aquaporin 4 inhibitors using in vitro and in silico methods. *Bioorg Med Chem* 2009;17:411-417.
11. Nakamura Y, Suzuki Y, Tsujita M, et al. Development of a novel ligand, [^{11}C]TGN-020, for aquaporin 4 positron emission tomography imaging. *ACS Chem Neurosci* 2011;2:568-571.
12. McCann J, Choi E, Yamasaki E, et al. Detection of carcinogens as mutagens in the Salmonella/microsome test: Assay of 300 chemicals. *Proc Natl Acad Sci USA* 1975;72:5135-5139.
13. Huber VJ, Tsujita M, Kwee IL, et al. Inhibition of aquaporin 4 by antiepileptic drugs. *Bioorg Med Chem* 2009;17:418-424.
14. Lu M, Lee MD, Smith BL, et al. The human AQP-4 gene: Definition of the locus encoding two water channel polypeptides in brain. *Proc Nat Acad Sci USA* 1996;93:10908-10912.
15. Amaya E, Musci TJ, Kirschner MW. Expression of a dominant negative mutant of the FGF receptor disrupts mesoderm formation in xenopus embryos. *Cell* 1991;66:257-270.
16. Francesca B, Rezzani R. Aquaporin and blood brain barrier. *Curr Neuropharmacol* 2010;8:92-96.
17. Speake T, Freeman LJ, Brown PD. Expression of aquaporin 1 and aquaporin 4 water channels in rat choroid plexus. *Biochim Biophys Acta* 2003;1609:80-86.
18. Tani T, Sakimura K, Tsujita M, et al. Identification of binding sites for anti-aquaporin 4 antibodies in patients with neuromyelitis optica. *J Neuroimmunol* 2009;211:110-113.